Rechargeable Lithium Battery Cathodes. Nonaqueous Synthesis, Characterization, and Electrochemical Properties of $LiCoO_2$

Timothy J. Boyle,* David Ingersoll,† Todd M. Alam,‡ Cory J. Tafoya, Mark A. Rodriguez,‡ Karel Vanheusden,§ and Daniel H. Doughty†

Advanced Materials Laboratory, Sandia National Laboratories, 1001 University Boulevard, SE, Albuquerque, New Mexico 87106, M.S. 0614 and M.S. 1407, Sandia National Laboratories, P.O. Box 5800, Albuquerque, New Mexico 87185, and US Air Force Research Laboratory, Kirtland Air Force Base, New Mexico 87117-5776

Received March 31, 1998. Revised Manuscript Received June 12, 1998

A nonaqueous coprecipitation process has been developed to prepare controlled stoichiometry lithium cobalt oxide precipitates. The process involved mixing a methanolic "$LiCo(NO_3)_3$" solution with a methanolic solution containing tetramethylammonium oxalate as a precipitating agent. The resulting oxalates were readily converted to phase-pure lithium cobalt oxide at 800 °C under an oxygen atmosphere. The various starting solutions, oxalate precipitates, and the resulting oxides have been extensively characterized using a variety of techniques, including multinuclear NMR, TGA/DTA, EPR, and XRD analyses. Results indicate that the strong interaction between the metals (Li and Co) that occurred in solution was maintained during precipitation. The calcined precipitate revealed that the desired $LiCoO_2$ phase was formed at 800 °C under an O_2 atmosphere. When electrochemically cycled, the material exhibited an initial capacity of ∼133 (mA h)/g with a fade of 0.02% in capacity per cycle.

Introduction

Batteries are prevalent throughout our society. Recent interest in high performance batteries has been driven by the development of miniature, portable electronic equipment and electric vehicles. Many battery types meet the output demands required for commercial use; however, the use of these batteries comes at the expense of the environment since heavy metals (i.e., Pb^{2+}, Cd^{2+}) are often a key component of these power sources. When disposed of in land fills, the heavy metals of these batteries often leak out of their casings and enter into the water table. In contrast, lithium batteries meet the commercial operating demands and are environmentally less damaging.[1−10] The majority of recent research concerning lithium-based batteries has focused on the so-called "rocking chair" materials or batteries that function by repeatedly cycling Li^+ between the cathode and anode.[1−10]

Each of the components (cathode, anode, and electrolyte) of rocking chair Li batteries have been extensively investigated for optimization of the capacity and cycleability. A significant number of recent studies have focused on the synthesis,[11−28] processing,[29−37] and/or

* To whom correspondences should be addressed.
† Sandia National Laboratories, M.S. 0614.
‡ Sandia National Laboratories, M.S. 1407.
§ Kirtland Air Force Base.

(1) Doughty, D. H. *SAMPE J.* **1996**, *32*, 75.
(2) Armstrong, R. A.; Bruce, P. G. *Nature* **1996**, *381*, 499.
(3) Thackeray, M. M. *J. Electrochem. Soc.* **1995**, *142*, 2558.
(4) Thackeray, M. M. *Prog. Solid State Chem.* **1997**, *25*, 1.
(5) Takehara, Z. *J. Power Sources* **1997**, *68*, 82.
(6) Banner, J. A.; Winchester, C. S. *J. Power Sources* **1997**, *65*, 271.
(7) Florjanczyk, Z.; Zygadlomonikowska, W.; Bzducha, W.; Borkowska, R. *Polimery* **1996**, *41*, 391.
(8) Salomon, M.; Scrosati, B. *Gazz. Chim. Ital.* **1996**, *126*, 415.
(9) Koksbang, R.; Barker, J.; Shi, H.; Saidi, M. Y. *Solid State Ionics* **1996**, *84*, 1.
(10) Ohzuku, T. *Lithium Batteries. New Materials, Developments and Perspectives*; Elsevier Science B. V.: Dordrecht, 1994.
(11) Zhecheva, E.; Stoyanova, R.; Gorova, M.; Alcantara, R.; Morales, J.; Tirado, J. L. *Chem. Mater.* **1996**, *8*, 1429.
(12) Schleich, D. M. *Solid State Ionics* **1994**, *70*, 407.
(13) Yazami, R.; Begrun, N.; Bonneau, M.; Molteni, M. *J. Power Sources* **1995**, *54*, 389.
(14) Pechini, M. U.S. Patent 3,330,697, 1967.
(15) Sankaranarayanan, V. K.; Pankhurst, Q. A.; P., D. D.; E. Johnson, C. E. *Magn. Magn. Mater.* **1994**, *130*, 288.
(16) Choy, J.-H.; Han, Y.-S.; Kim, J.-T.; Kim, Y.-H. *J. Mater. Chem.* **1995**, *5*, 57.
(17) Douy, A.; Odier, M. *Mater. Res. Bull.* **1989**, *24*, 1119.
(18) Baythourn, M. S. G.; Sale, F. R. *J. Mater. Sci.* **1982**, *17*, 2757.
(19) Anderton, D. J.; Sale, F. R. *Powder Metall.* **1978**, *22*, 14.
(20) Hennings, D.; Mayr, W. *J. Solid State Chem.* **1978**, *26*, 329.
(21) Johnston, W. D.; Heikes, R. P.; Sestrich, D. *J. Phys. Chem. Solids* **1985**, *7*, 1.
(22) Orman, H. J.; Wiseman, P. J. *Acta Crystallogr.* **1985**, *C40*, 12.
(23) Amatucci, G. G.; Tarascon, J. M.; Klein, L. C. *Solid State Ionics* **1996**, *83*, 167.
(24) Chen, C. H.; Buysman, A. A. J.; Kelder, E. M.; Schoonman, J. *Solid State Ionics* **1995**, *80*, 1.
(25) Banov, B.; Bourilkov, J.; Mladenov, M. *J. Power Sources* **1995**, *54*, 268.
(26) Caurant, D.; Baffier, N.; Garcia, B.; Pereiraramos, J. P. *Solid State Ionics* **1996**, *91*, 45.
(27) Lundblad, A.; Bergman, B. *Solid State Ionics* **1997**, *96*, 172.
(28) Gilmour, A. *J. Power Sources* **1997**, *65*, 241.
(29) Sheu, S. P.; Yao, C. Y.; Shen, J. M.; Chiou, Y. C. *J. Power Sources* **1997**, *68*, 533.
(30) Chang, H. S. W.; Lee, T. J.; Lin, S. C.; Jeng, J. H. *J. Power Sources* **1995**, *54*, 403.
(31) Wang, B.; Bates, J. B.; Hart, F. X.; Sales, B. C.; Zuhr, R. A.; Robertson, J. C. *J. Electrochem. Soc.* **1996**, *143*, 3203.
(32) Striebel, K. A.; Deng, C. Z.; Wen, S. J.; Cairns, E. J. *J. Electrochem. Soc.* **1996**, *143*, 1821.

S0897-4756(98)00208-7 CCC: $15.00
Published on Web 07/23/1998

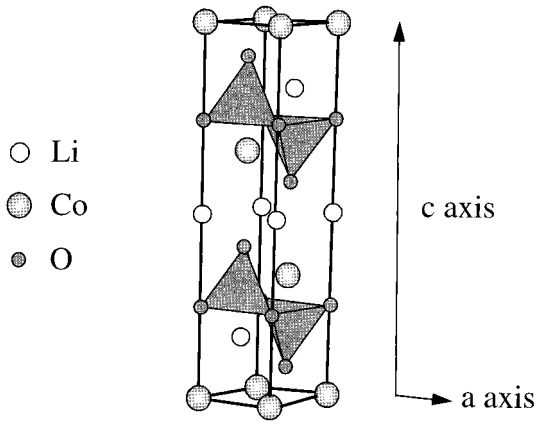

Figure 1. Schematic representation of $LiCoO_2$.

electrochemical identification[32−34,38−46] of cathode materials. Only three materials are usually identified as suitable for use as cathodes in 4 V lithium batteries: the spinel phase of $LiMn_2O_4$ and the layered $LiCoO_2$ and $LiNiO_2$ compounds.[1−10] $LiMn_2O_4$ is attractive since it is relatively inexpensive and environmentally benign but suffers from low theoretical capacity. We have investigated this material and developed a novel route for the synthesis of various $Li_xMn_2O_4$ phases.[47,48] In the process of this investigation we also attempted to synthesize the other rocking chair cathodes. In this paper we describe application of this process to the production of high-quality $LiCoO_2$ materials.

Figure 1 shows a schematic representation of $LiCoO_2$.[49] Classical approaches to generate this material involve dry-mixing of lithium and cobalt salts followed by high-temperature processing.[21,22] Solution routes that use acetate-, citrate-, and glycolate-ligated precursors have been developed which allow for greater homogeneity and lower processing temperatures.[11−20] Using our nonaqueous route for the production of $Li_xMn_2O_4$ materials, we have also been able to generate phase pure $LiCoO_2$. This paper reports on the synthesis, characterization, and the electrochemical properties of the $LiCoO_2$ material produced by this method.

Experimental Section

All reactions were performed under dry nitrogen or argon, using standard Schlenk, vacuum line, and glovebox techniques. MeOH was dried and distilled from CaH_2 immediately prior to use, whereas the following compounds were used as received (Aldrich): lithium nitrate ($LiNO_3$), cobalt(II) nitrate ($Co(NO_3)_2$), tetramethylammonium hydroxide [$(Me_4N)(OH)$], oxalic acid ($H_2C_2O_4$), $LiPF_6$ (Hashimoto), Teflon (DuPont), polyvinyl difluoride (PVDF, Solvay and Elf Atochem), ethylene carbonate (EC, Merck), and dimethyl carbonate (DMC, Merck). After stirring for 12 h, $(Me_4N)_2(C_2O_4)$ was isolated from the reaction mixture of $H_2C_2O_4$ and 2 equiv of $(Me_4N)(OH)$ in MeOH, by removal of all of the volatile material.[47,48]

Solution ^{7}Li, ^{15}N, and ^{59}Co NMR spectral data were recorded on a Bruker DMX 400 using a 5 mm broadband probe at resonant frequencies of 155.5 MHz for ^{7}Li, 40.53 MHz for ^{15}N, and 94.95 MHz for ^{59}Co. All experiments were performed at 298 K unless otherwise noted. Chemical shifts for ^{7}Li,^{15}N, and ^{57}Co NMR spectra were referenced against external 1 M LiCl in D_2O (δ 0.0 ppm), CH_3NO_2 (δ 381.0 ppm), and $K_3[Co(CN)_6]_3$ in D_2O (δ 0.0 ppm), respectively. The ^{15}N spectra were obtained using an inverse gated pulse sequence to reduce negative NOE effects. Solid-state NMR spectra were recorded on an AMX 400 using a 4 mm MAS broadband probe with spinning frequencies ranging between 12 and 12.5 kHz, using $\pi/12$ pulses to reduce quadrupolar mutation effects. The resonant frequencies for ^{6}Li was 58.88 MHz, ^{7}Li was 155.5 MHz, and ^{57}Co was 94.95 MHz. ^{6}Li and ^{7}Li chemical shifts were reference to external 1 M LiCl in D_2O (δ 0.0 ppm) and ^{57}Co with respect to solid $K_3[Co(CN)_6]_3$ (δ 0.0 ppm).

Thermal gravimetric analysis/differential thermal analysis (TGA/DTA) experiments were performed on 10−15 mg of the appropriate powder using a Polymer Laboratories STA 1500 Instrument under an atmosphere of oxygen. X-ray diffraction analysis was performed using a Siemens automated $\theta-2\theta$ powder diffractometer equipped with Cu Kα radiation, a diffracted-beam graphite monochromator, and scintillation counter. Electron paramagnetic resonance (EPR) studies were performed at 15 K using a Bruker Instruments X-band spectrometer.

$LiCoO_2$.[47,48] A maroon solution of $Co(NO_3)_2$ (2.01 g, 6.90 mmol) in MeOH (∼6 mL) was combined with a clear solution of $LiNO_3$ (0.50 g, 6.90 mmol) in ∼6 mL MeOH (*note*: A slight excess of $LiNO_3$ was added to compensate for Li loss during processing). There was no noticeable change in color or clarity of the solution. After stirring for 5 min, $(Me_4N)_2C_2O_4$ (4.30 g, 20.7 mmol) in MeOH (∼10 mL) was then added to this mixture and a bright pink precipitate immediately formed. The volatile material was then removed by rotary evaporation. An FT-IR pattern of the prefired powder is supplied for identification: FT-IR (KBr, cm^{-1}) 3417 (w), 3032 (w), 2966 (w), 2919 (w), 2376 (w), 1613 (br, s), 1487 (s), 1341 (sb), 1096 (w), 1023 (w), 950 (s), 831 (m), 798 (m), 777 (w). In a muffle furnace, the pink powder was heated in air to 300 °C at a ramp rate of 0.1 °C/min followed by another heat treatment in a tube furnace to 800 °C at 5 °C/min under O_2 for 24 h. From a preweighed sample of 5.43 g, 0.59 g of calcined material was isolated. XRD analysis of this black-blue powder proved it was phase-pure $LiCoO_2$.

Electrochemical Characterization. Porous electrodes were prepared using the $LiCoO_2$ oxide powder having a nominal composition of 82% active material (the oxide), 10% Schwennigan acetylene black carbon (SAB, added for electronic conductivity), and 8% binder (Teflon or PVDF). To prepare the electrodes, SAB and the $LiCoO_2$ oxide powder were milled for 20 min, followed by mixing with the appropriate binder. When Teflon was used as the binder, a dry blending technique was employed and an electrode was pressed from this mixture.

(33) Takada, K.; Aotani, N.; Iwamoto, K.; Kondo, S. *Solid State Ionics* **1995**, *79*, 284.
(34) Fragnuaud, P.; Brousse, T.; Schleich, D. M. *J. Power Sources* **1996**, *63*, 187.
(35) Huang, W. W.; Frech, R. *Solid State Ionics* **1996**, *86*, 395.
(36) Chen, C. H.; Kelder, E. M.; Jak, M. J. G.; Schoonman, J. *Solid State Ionics* **1996**, *86*, 1301.
(37) Marini, A.; Berbenni, V.; Massarotti, V.; Capsoni, D.; Antolini, E. *J. Solid State Chem.* **1995**, *116*, 15.
(38) Saito, Y.; Kanari, K.; Takano, K. *J. Power Sources* **1997**, *68*, 451.
(39) Arai, H.; Okada, S.; Sakaurai, Y.; Yamaki, J. *Solid State Ionics* **1997**, *95*, 275.
(40) Kim, H. S.; Cho, B. W.; Kim, J. T.; Yun, K. S.; Chun, H. S. *J. Power Sources* **1996**, *62*, 21.
(41) Nohma, T.; Kurokawa, H.; Uehara, M.; Takahashi, M.; Nishio, K.; Saito, T. *J. Power Sources* **1995**, *54*, 522.
(42) Yazami, R.; Lebrun, N.; Bonneau, M.; Molteni, M. *J. Power Sources* **1995**, *54*, 389.
(43) Barker, J.; Pynenburg, R.; Koksbang, R.; Saidi, M. Y. *Electrochim. Acta* **1996**, *41*, 2481.
(44) Rahner, D.; Machill, S.; Schlorb, H.; Siury, K.; Kloss, M. *Solid State Ionics* **1996**, *86−8*, 891.
(45) Marini, A.; Berbenni, V.; Massarotti, V.; Capsoni, D.; Bruni, G. *Zeits. Naturforsch. Sec. A- A J. Phys.* **1996**, *51*, 813.
(46) Rabou, L. P. L. M.; Roskam, A. *J. Power Sources* **1995**, *54*, 316.
(47) Boyle, T. J.; Voigt, J. A. In Section 52−2 (Electrochemical, Radiational, and Thermal Energy Technology): US 5630994, 1997; p 6.
(48) Voigt, J. A.; Boyle, T. J.; Doughty, D. H.; Johnson, B.; Levy, S. C.; Hernandez, B. A.; Tafoya, C. J.; Rosay, M. *Materials Research Society Symposium Proceedings;* San Fransisco, **1995**, 393, 101.
(49) Antaya, M.; Cearns, K.; Preston, J. S.; Reimers, J. N.; Dahn, J. R. *J. Appl. Phys.* **1994**, *76*, 2799.

In the case when PVDF was used as the binder, the oxide/carbon mixture was dispersed in a solution of the PVDF dissolved in dimethyl formamide and then cast directly onto an aluminum grid that was used as the current collector. The electrodes were dried in a vacuum oven (1×10^{-2} Torr) at 60 °C for 12 h or longer.

Three electrode cells were assembled using reference electrodes composed of lithium metal. The working and counter electrodes were separated from one another in the stack using one mil Celgard separator and a Swagelok fitting made from PFA as the cell holder. Stainless steel and aluminum posts were used to provide electrical contact to the lithium and oxide, respectively. After assembly, a vacuum (5×10^{-5} Torr) was applied to the cells and maintained for at least 10 min, followed by introduction of the electrolyte solution (vide supra). This was undertaken to ensure complete filling of the porous network of the electrode and separators. The solvent system used to fill the cells consisted of 1 M $LiPF_6$ in a 50/50 mixture of EC/DMC.

Electrochemical cycling of the cells was performed using a taper charge to 4.3 V at an initial current density of 0.5 mA/cm^2. The discharge was performed at a current density of 0.5 mA/cm^2, to a final voltage end condition of 3.5 V. A total of five cycles were completed using these initial current densities. To evaluate the rate capability of the materials, current densities of 1 and 3 mA/cm^2 were also used. This was followed by repetitive cycling at 0.5 mA/cycle in order to assess the long-term stability characteristics of the materials.

Results and Discussion

Synthesis. Our previously reported method for production of $Li_xMn_2O_4$ was slightly modified for the production of $LiCoO_2$.[47,48] To a maroon $Co(NO_3)_2$/MeOH solution was added a clear $LiNO_3$/MeOH solution with stirring (eq 1). After 5 min, dehydrated oxalic acid [$(Me_4N)_2(C_2O_4)$] in MeOH was added to this reaction mixture to produce an oxalate precipitate (eq 2). The insoluble product was dried in vacuo. This powder was handled under an inert atmosphere due to its sensitivity to atmospheric moisture.

$$LiNO_3 + Co(NO_3)_2 \xrightarrow{MeOH} \text{“}LiCo(NO_3)_3 \quad (1)$$

$$\text{“}LiCo(NO_3)_3\text{”} + 3(Me_4N)_2(C_2O_4) \xrightarrow[-3[O_3N][NMe_4]]{MeOH} \text{“}LiCo(C_2O_4)_{1.5} \quad (2)$$

$$\text{“}LiCo(C_2O_4)_{1.5}\text{”} \xrightarrow{\Delta} LiCoO_2 \quad (3)$$

The metallo-organic precursor was converted to the desired oxide phase (eq 3) using a slow heating cycle under a controlled atmosphere.[47,48] This was found to be the optimal method to eliminate “hot spots” during oxalate decomposition, noted as large exotherms in the thermal analysis.[47,48] Initial heating occurred under atmospheric conditions at a rate of 0.1 °C/min up to 300 °C in an alumina tray in a box furnace. The subsequent heat treatment continued in an alumina tray in a tube furnace up to 800 °C at 5°/min under an atmosphere of O_2 with a 24 h hold time at this temperature, resulting in a black-blue material.

Characterization. In an effort to determine the homogeneity of the precursor solutions as well as the resulting precipitate, investigations of the individual compounds ($LiNO_3$ and $Co(NO_3)_2$), the resulting mixture (“$LiCo(NO_3)_3$” in MeOH), and precipitates (“Li-ox”, “Co-ox”, and “LiCo-ox”: ox = oxalate) were undertaken.

Table 1. FT-IR and NMR Spectral Data for $LiNO_3$, $Co(NO_3)_3$, $LiCo(NO_3)_3$, $LiNO_3 + (Me_4N)_2(C_2O_4)$, $Co(NO_3)_3 + (Me_4N)_2(C_2O_4)$, $Co(NO_3)_3$, and $LiCo(NO_3)_3 + 3(Me_4N)_2(C_2O_4)$

nitrates	FT-IR NO_3 stretches[a]	solution NMR shifts (ppm) ^{7}Li[b]	^{15}N[c]
$LiNO_3$	1633, 1388, 1354, 1262	0.2	377
$Co(NO_3)_2$	1627, 1388, 1355	3.1	390
$LiCo(NO_3)_3$	1633, 1388, 1355, 1262		

oxalates	FT-IR C=O stretches[a]	^{7}Li MAS NMR shifts (ppm)[b]
$LiNO_3 + (Me_4N)_2(C_2O_4)$	1613, 1560, 1489, 1334, 1316, 1298	2.7, 1.2, 0.1
$Co(NO_3)_2 + (Me_4N)_2(C_2O_4)$	1626, 1487, 1361, 1308	
$LiCo(NO_3)_3 + 3(Me_4N)_2(C_2O_4)$	1613, 1487, 1341	−4.2, −5.0

[a] FT-IR stretches (1700−1200 cm^{-1}). [b] Referenced to external 1 M LiCl (δ 0.0 ppm). [c] Referenced to neat CH_3NO_3 (δ 381 ppm).

These studies included NMR (solution and solid state) spectroscopy, FT-IR spectroscopy, thermal analysis (TGA/DTA), and electron paramagnetic resonance (EPR) spectroscopy. The various chemical components of this process has been broken up into three sections for discussion purposes: the precursor solution behavior, the oxalate precipitation product (LiCo-ox), and the calcined $LiCoO_2$ material.

(i) Precursor Solution. Two analytical methods were undertaken to determine the homogeneity of the $LiCo(NO_3)_3$ in MeOH precursor solution: FT-IR and solution NMR. The major FT-IR spectral stretches for $LiNO_3$, $Co(NO_3)_2$, and precursor solution of $LiCo(NO_3)_3$ which had been dried to a powder are tabulated in Table 1. As noted, the shifts for the NO_3 stretches of the $LiCo(NO_3)_3$ mixture powder are only slightly altered in comparison to the individual starting materials. Therefore, it was not possible to define the degree of mixing that the solution had undergone. Fortunately, the precursor solution generated in eq 1 possesses a wide number of accessible NMR (^{7}Li, ^{15}N, and ^{59}Co) nuclei.[50] The NMR data collected for this precursor solution are also tabulated in Table 1. NMR spectra were obtained on the nitrate precursors [$LiNO_3$, $Co(NO_3)_2$] and the precursor solution [“$LiCo(NO_3)_3$”] to infer solution interactions.

The ^{7}Li NMR spectrum obtained on the $LiNO_3$ precursor in MeOH revealed an extremely sharp resonance at δ 0.2 ppm. Upon mixing to form the $LiCo(NO_3)_3$ precursor solution, there was a significant downfield shift in the resonance to δ 3.1 ppm with no evidence of the original δ 0.2 ppm resonance. This indicates that the paramagnetic Co metal center in the $LiCo(NO_3)_3$ solution is uniformly influencing the Li metal center, resulting in a homogeneous interaction within the solution. This homogeneity was further verified by the shift observed for the ^{15}N NMR resonances. The ^{15}N chemical shifts for $LiNO_3$ change from δ 377 to 390 ppm upon mixing with $Co(NO_3)_2$ to form $LiCo(NO_3)_3$. No ^{15}N

(50) Chemical and Biological Applications. *NMR of Newly Accessible Nuclei*; Academic Press: New York, 1983; Vol. 1, p 298.

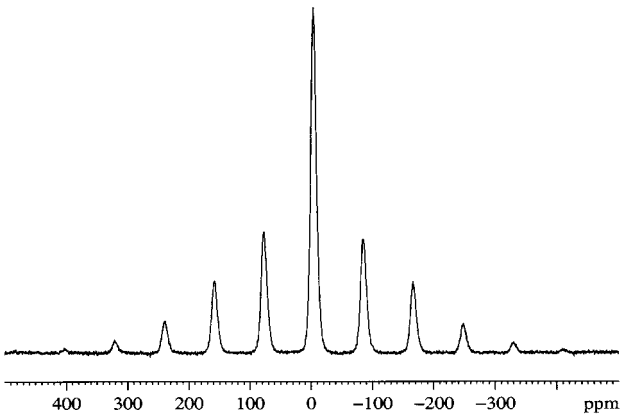

Figure 2. The solid-state ^{7}Li MAS NMR spectrum of LiCo-ox precipitate ($LiCo(O_4C_2)_{1.5}$).

resonance was observed for the $Co(NO_3)_2$ precursor, due to the paramagnetic nature of the Co^{2+} metal center. The shift in the ^{15}N resonances from the starting material to the mixed complex indicates that the NO_3 of the Li metal centers have some interaction with the Co^{2+} metal center. Because no ^{15}N signal was observed for $Co(NO_3)_2$ (which contains a direct (NO_3)-Co bond), the ^{15}N resonance observed in the $LiCo(NO_3)_3$ mixture is assumed to result from NO_3 groups that are not either bridging or directly bound to the Co^{2+} metal center. Due to the highly asymmetric ligand arrangement around the metal center or paramagnetic effects, neither $Co(NO_3)_2$ nor $LiCo(NO_3)_3$ yielded a ^{59}Co NMR signal.

(ii) Oxalate Precipitate. On the basis of the ^{7}Li and ^{15}N NMR data, the solution generated in eq 1 was homogeneous with a strong interaction between the Li and Co through some form of NO_3 linkage. However, it was necessary to prove that the uniform nature of the precursor solution was retained upon precipitation (eq 2). Therefore, several studies concerning the solid precipitate were undertaken including FT-IR, solid-state NMR, TGA/DTA, and EPR.

FT-IR spectra of Li-ox and Co-ox were obtained from the precipitation of $LiNO_3$ or $Co(NO_3)_2$ in analogous manner, as shown in eq 2. The C═O stretches of the Li-ox and Co-ox material had stretches at 1610 and 1550 cm^{-1} and 1610 and 1498 cm^{-1}, respectively; however, the LiCo-ox precipitate had C═O stretches at 1605 and 1500 cm^{-1}. These spectra clearly show that the new precipitate is not composed of the individual components but is a homogeneous mixed cation powder. This idea was further verified by solid-state NMR spectroscopy.

The ^{6}Li, ^{7}Li, and ^{57}Co solid-state MAS NMR investigations were undertaken for Li-ox, Co-ox, and LiCo-ox to further elucidate the homogeneity of the resultant precipitate. The results of these multinuclear NMR investigations are metrically tabulated in Table 1. The solid-state ^{7}Li NMR spectrum for the LiCo-ox precipitate is shown in Figure 2. Due to the difficult observation of natural abundance ^{15}N NMR signals in the solid state, these investigations were not pursued.

The solid-state MAS NMR spectra obtained for ^{7}Li (the nuclear spin $I = {}^3/_2$) in these samples is composed of an isotropic resonance resulting from the $\pm{}^1/_2 \leftrightarrow \pm{}^1/_2$ transition, with the spinning sidebands resulting from $\pm{}^3/_2 \leftrightarrow \pm{}^1/_2$ transitions. For the small quadrupolar interaction, the first-order shift on the central $\pm{}^1/_2 \leftrightarrow \pm{}^1/_2$ transition is zero, while for the larger quadrupolar interaction a second-order quadrupolar shift ($\delta_{iso}^{(2Q)}$) may be observed, such that the observed shift (δ^{obs}) is the sum of the true chemical shift (δ^{CS}) and this quadrupolar shift (eq 4).[51] In eqs 4 and 5, the parameters I, m, C_Q, η_Q are defined as the spin number, the energy level, the quadrupolar coupling constant, and the asymmetry parameter, respectively, while ν_L is the Larmor frequency.[51] For ^{6}Li, which is a $I = 1$ nuclei, only a single transition is observed, resulting from the $\pm1 \leftrightarrow 0$ transition, and the second-order quadrupolar shift can be neglected[52] such that the observed shift is close to the isotropic chemical shift (i.e., $\delta_{iso}^{(2Q)} \sim 0$).

$$\delta_{iso}^{(2Q)} = -\frac{3}{40}\frac{C_Q^2}{\nu_L^2}\frac{[I(I+1) - 3 - 9m(m-1)]}{I^2(2I-1)^2}\left(1 + \frac{\eta_Q^2}{3}\right) \times 10^6 \quad (4)$$

$$\delta^{obs} = \delta^{CS} + \delta_{iso}^{(2Q)} \quad (5)$$

Since ^{6}Li and ^{7}Li are expected to have the same chemical shift, any differences must be due to the second-order quadrupolar shift in ^{7}Li, as given by eqs 4 and 5 in ppm. For the Li-ox, a central ^{7}Li resonance was observed at δ 2.7 ppm with minor resonances noted at 1.2 and 0.1 ppm. The ^{6}Li NMR spectra revealed the major resonance as δ 2.7 ppm with only a single minor resonance at 1.4 ppm. The difference in the ^{6}Li and ^{7}Li chemical shift for the major resonances of Li-ox suggests that the quadrupolar interaction ($\delta_{iso}^{(2Q)}$) is very small. This is confirmed by ^{6}Li and ^{7}Li MAS experiments performed at a lower Larmor frequency, where the observed chemical shift was also δ 2.7 ppm. Note that the quadrupolar shift $\delta_{iso}^{(2Q)}$ in eq 4 has a $1/\nu_L^2$ field dependence. For the LiCo-ox material the central ^{7}Li NMR resonance at δ −4.2 ppm was observed at 155.5 MHz and was ∼10 ppm wider than the ^{7}Li signal observed in the Li-ox species. The ^{6}Li MAS spectra for the LiCo-ox was not observable at either field strength due to extreme broadening of the resonance. The observed central transition frequency for subsequent ^{7}Li MAS NMR experiments at 116.6 MHz was δ −6.7 ppm, clearly showing that the second-order quadrupolar shift ($\delta_{iso}^{(2Q)}$) is *not* negligible for the LiCo-ox complex. Using the field dependence of the observed shift and eqs 4 and 5 above, the true chemical shift and quadrupolar product were estimated to be $\sim\delta^{CS}$ 0.99 ppm and $P_Q^2 \sim$ 1.7 MHz, where $P_Q = C_Q\,(1 + \eta_Q^2/3)^{1/2}$. The chemical shift change between Li-ox and LiCo-ox was ∼3.7 ppm out of a total ^{7}Li chemical shift dispersion of ∼10 ppm. The appearance of a considerable quadrupolar interaction of 1.7 MHz for the LiCo-ox precursor suggests a direct interaction between the Li and Co nuclei with a significant change in the electrical field gradient around the Li nucleus. Furthermore, the precipitate must be a homogeneous mixture and not a phase-separated mixture. ^{57}Co NMR revealed a very sharp distinct

(51) Massiot, D.; Bessada, C.; Coutures, J. P.; Taulelle, F. *J. Magn. Resonance* **1990**, *90*, 231.
(52) Xu, Z.; Stebbins, J. F. *Solid State Nuclear Magn. Res.* **1995**, *5*, 103.

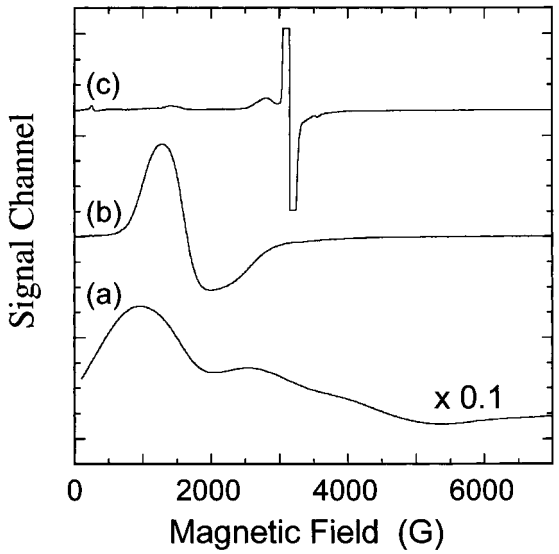

Figure 3. The EPR spectrum of (a) $Co(NO_3)_2$, (b) LiCo-ox precipitate, and (c) $LiCoO_2$.

isotropic resonance for the standard. However, for both the Co-ox and LiCo-ox precipitate, only very broad signals of widths on the order of ~2000 ppm were observed and they provided little information.

The FT-IR and NMR data indicated that the solution homogeneity observed by NMR analysis was carried over upon precipitation. The homogeneity of the powder was further verified by the thermal analysis of the individual oxalate precursors (Li-ox and Co-ox) and the mixed oxalate (LiCo-ox) precursor. Each of these materials was analyzed by TGA/DTA. The individual components showed decomposition temperatures (thermal events) at ~319 °C (exo) and ~243 °C (exo) for the Li-ox and Co-ox individual precipitates, respectively. Furthermore, mixing of the individual powders in a 1:1 ratio revealed exothermic weight losses at ~326 and 260 °C. In contrast, the precipitated LiCo-ox mixture showed three exothermic peaks at ~207, 243 (major), and 263 °C. This indicates that the LiCo-ox precipitate is a complex homogeneous mixture not merely the coprecipitated individual components. Furthermore, as was noted for the $LiMn_2O_4$ system, large exotherms occurred for the precipitated material during decomposition. To minimize the generation of "hot spots" that can form during the exothermic decomposition, slow heating ramp rates were used.

EPR analysis was undertaken to elucidate the general constructs of the precipitate powder by determining the symmetry and the oxidation state of the Co^{2+} cation after precipitation. At 15 K, the $Co(NO_3)_2$ precursor (Figure 3a) shows a very strong Co^{2+} EPR line.[53] In exact octahedral symmetry, the $3d^7$ electronic configuration has an orbital triplet as its lowest energy state that is split by spin−orbit coupling, resulting in a Kramers doublet with $\mathbf{g} = 4.33$.[53] Deviations from the octahedral symmetry strongly mix the next excited states, which have only slightly higher energies, and the ground-state **g** tensor becomes anisotropic. The resonance spectrum for Co^{2+} in $Co(NO_3)_2$ indicates that the Co^{2+} cation resides in a site of slightly lower than ideal

(53) Harris, E. A. *Phys. Chem. Glasses* **1987**, *28*, 196.

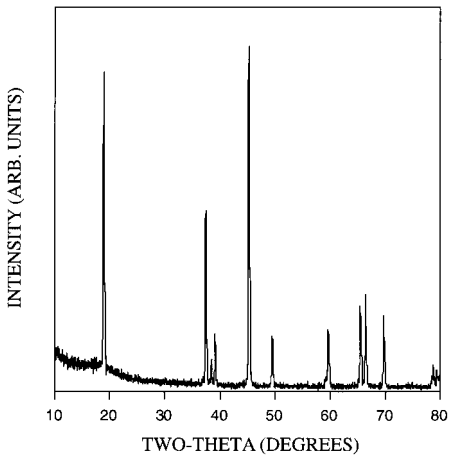

Figure 4. XRD spectrum of $LiCoO_2$ powder (PDF card #44-145).

symmetry. This would be consistent with the lack of observed ^{15}N and ^{57}Co NMR signal for this compound. In the mixed LiCo-ox precipitate, the Co^{2+} powder EPR spectrum (Figure 3b) is significantly altered from the $Co(NO_3)_2$ spectrum. This spectrum indicates that the distorted octahedral symmetry observed for $Co(NO_3)_2$ has changed to reflect a Co^{2+} cation site with strong octahedral symmetry. The density of Co^{2+} in the resulting mixed LiCo-ox precipitate is approximately 2 orders of magnitude lower than that in $Co(NO_3)_2$, which is a reflection of the significant amount of organic and inorganic components present upon precipitation. On the basis of the above data, the Co^{2+} starting cation maintains its oxidation state throughout the precipitation process.

(iii) Calcined Material. Upon heating, under the appropriate conditions (800 °C under O_2), the stoichiometric precipitate powder is converted into the high-temperature form (HT)[49] of $LiCoO_2$ and a minor phase of Co_3O_4. In the HT-$LiCoO_2$ structure, Li and Co alternate octahedral coordinated layers. Figure 1 displays one unit cell for the structure; the oxygens are plotted as tetrahedrons around the Li and Co to illustrate that part of the octahedral oxygen framework surrounds the cations. The structure displays a trigonal $R\bar{3}m$ space group where Co is located at (0, 0, 0) or the 3a site, Li is located at (0, 0, 0.5) or the 3b site, and O is locate at (0, 0, 0.25) or the 6c site. The XRD data (Figure 4) was refined to obtain lattice parameters of $a = 2.816(3)$ Å and $c = 14.058(9)$ Å.

In the synthesis of Li_xCoO_2, excess lithium ($x = 1.05$, 1.10, 1.15) was added to compensate for any material lost during the thermal processing. The resultant material was found to be consistent with phase-pure $LiCoO_2$ material (see Figure 4). This addition eliminated any of the Co_3O_4 material that had been present at a 1:1 stoichiometry. However, the detection of excess Li compounds within the diffraction data (i.e., Li_2O or Li_2CO_3) would be extremely difficult due to the lack of scatter associated with the Li atom. Therefore, only a slight excess of $LiNO_3$ (which subsequently proved to be sufficient) was added to the precursor solution to ensure a phase-pure material.

An EPR spectrum was then obtained on the phase-pure calcined material. Co^{3+} is EPR inactive and no signal should be observed. As can be observed in Figure

3c, the strong Co^{2+} signal is no longer present in any significant quantities. The narrow line (truncated) located in the center of the spectrum is a result of an impurity present (starting material is +98% pure). On the basis of its EPR signature and the nature of Co,[54] this signal most likely represents either Ni or Cr cations. None-the-less, the resultant spectrum indicates that the majority of the sample has been converted to the Co^{3+} oxidation state, which is consistent with the formation of $LiCoO_2$.

Electrochemical Properties. On the basis of the above analytical data, it is apparent that the $LiCo(NO_3)_3$ solution was a homogeneous mixture which maintained its intimate mixing upon precipitation as LiCo-ox. After processing to the phase-pure $LiCoO_2$ material, the electrochemical behavior of this material was evaluated using a three-electrode cell that employed lithium reference and counter electrodes under a variety of conditions (i.e., discharge rates and final charge voltage).

The first cycle discharge capacity of the $LiCoO_2$ material upon charging to 4.1 V (vs Li°) at 0.5 mA/cm^2 was ~90 (mA h)/g. When charged to 4.35 V and discharged at 0.5 mA/cm^2, the initial reversible capacity is higher than when charged at 4.1 V and was found to be ~133 (mA h)/g. The theoretical value for full removal of the Li ions is 273.67 (mA h)/g; however, a practical limitation of a little over half of the lithium ions can actually be removed, thus limiting the usable capacity to ~160 (mA h)/g.[55] The charge/discharge profile of the material when charged to 4.35 V is shown in Figure 5a. As can be discerned, the discharge curve is relatively flat, which is consistent with other reports.[55] Additional capacity can be obtained by cycling to even higher voltages; however, significant fade is observed under these conditions. This loss of capacity presumably results from the instability of the lattice (Figure 1) as a result of the intercalation/deintercalation of lithium atoms during cycling. The discharge capacity as a function of cycle number was also evaluated for each charge voltage for up to 100 cycles, and the data obtained for one of the cells was cycled to 4.35 V (Figure 5b). The cycle-to-cycle fade rate is on the order of 0.02% per cycle, which is consistent with other literature reports.[55]

We have also performed an initial evaluation of the rate capability of these materials, performed at rates of 0.5, 1, and 3 mA/cm^2 during the initial cycling of the material. The behavior can be seen in parts b and c of Figure 5, the latter of which shows comparative plots of the charge/discharge curves for these materials at the different rates studied. As expected, the relative capacities for higher discharge rates are less than those observed at lower rates.

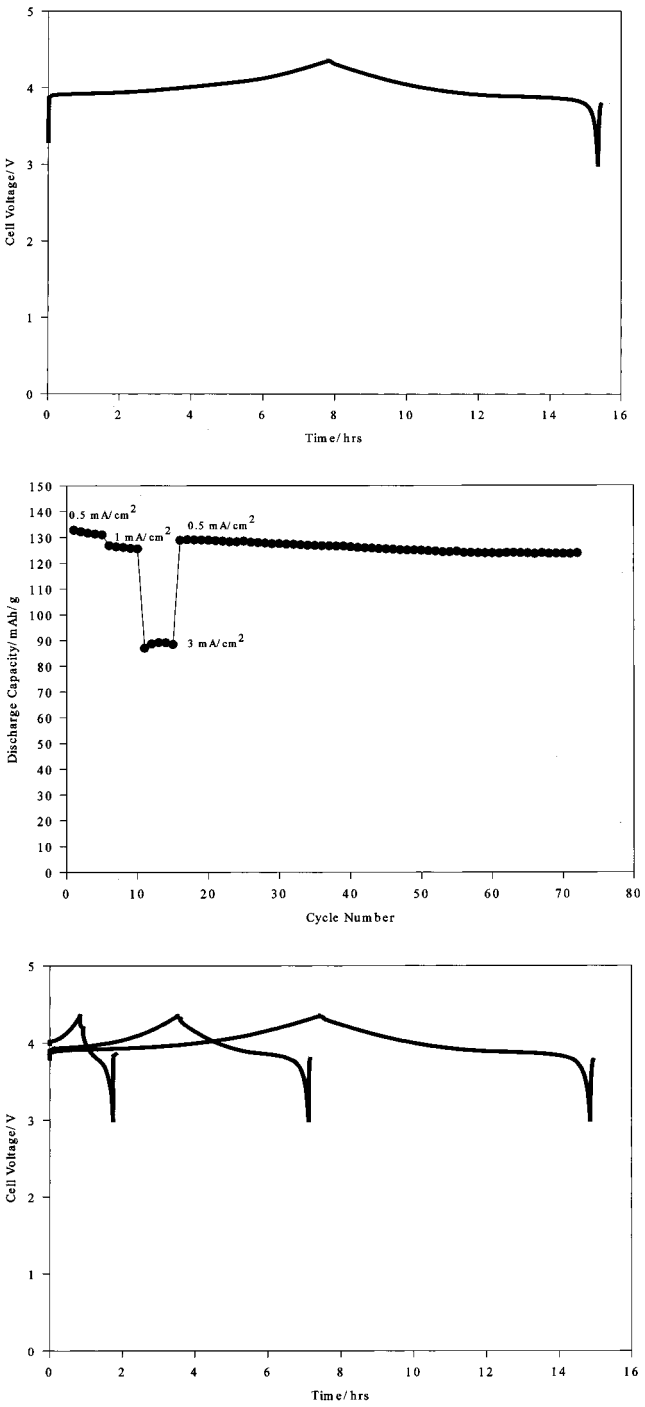

Figure 5. Battery results: (a) initial charge/discharge profile for $LiCoO_2$ at current densities of 0.5 mA/cm^2, (b) discharge capacity as a function of cycle number and discharge rates for $LiCoO_2$ charged to 4.35 V (The first five cycles and remaining cycles beginning with cycle 16 were discharged at 0.5 mA/cm^2. Cycles 6−10 and 11−15 were performed at discharge rates of 1 and 3 mA/cm^2, respectively.), and (c) comparative charge/discharge profiles for $LiCoO_2$ at rates of 0.5, 1, and 3 mA/cm^2.

Conclusion

A nonaqueous solution route for production of $LiCoO_2$ has been determined. The precursor solution ($LiNO_3$/$Co(NO_3)_2$/MeOH) was found by multinuclear NMR analysis to be a homogeneous mixture. Precipitation by addition of dehydrated oxalic acid yields a homogeneous powder, as observed by multinuclear solid-state NMR, TGA/DTA, and FT-IR. EPR studies indicate that the Co^{2+} oxidation state of the starting material is maintained upon precipitation but is altered to Co^{3+} during calcination. XRD studies indicate that mixed phases were isolated unless excess lithium was added to compensate for Li volatilization. The resulting $LiCoO_2$ has capacities of ~133 mA/h and a fade of 0.02%

(54) Cotton, F. A.; Wilkinson, G. *Advanced Inorganic Chemistry*, 5th ed.; John Wiley & Sons: New York, 1988; pp 724−741.

(55) Abraham, K. M.; Pasquariello, D. M.; Willstaedt, E. M. *J. Electrochem. Soc.* **1998**, *145*, 482.

per cycle for the test cell conditions we have investigated. There has been some variability in performance characteristics between samples which is not fully understood to date. Doping of the $LiCoO_2$ material is possible by this simple route and the resulting materials show promise for increasing the capacity of the resultant material.

Acknowledgment. This work supported by the United States Department of Energy under contract number DE-AC04-94AL85000. Sandia is a multiprogram laboratory operated by Sandia Corp., a Lockeed Martin Co., for the United States Department of Energy.

CM9802088